LANGMUIR Article
Cite This: *Langmuir* 2018, 34, 10806−10815
pubs.acs.org/Langmuir

Characterization of *Pseudomonas aeruginosa* Films on Different Inorganic Surfaces before and after UV Light Exposure

Alexey V. Gulyuk,[†] Dennis R. LaJeunesse,[‡] Ramon Collazo,[†] and Albena Ivanisevic*[,†]

[†]Department of Materials Science and Engineering, North Carolina State University, Raleigh, North Carolina 27695, United States
[‡]Joint School of Nanoscience and Nanoengineering, University of North Carolina-Greensboro and North Carolina A&T State University, Greensboro, North Carolina 27401, United States

Supporting Information

ABSTRACT: The changes of the surface properties of Au, GaN, and SiO_x after UV light irradiation were used to actively influence the process of formation of *Pseudomonas aeruginosa* films. The interfacial properties of the substrates were characterized by X-ray photoelectron spectroscopy and atomic force microscopy. The changes in the *P. aeruginosa* film properties were accessed by analyzing adhesion force maps and quantifying the intracellular Ca^{2+} concentration. The collected analysis indicates that the alteration of the inorganic materials' surface chemistry can lead to differences in biofilm formation and variable response from *P. aeruginosa* cells.

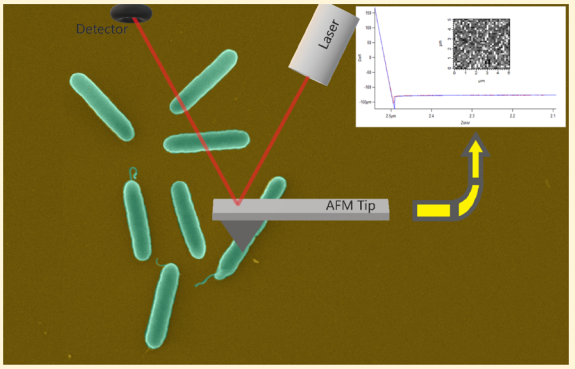

INTRODUCTION

Modern computing technology is approaching limits of exponential development, and various paradigms to overcome existing limitations have been proposed, including quantum computing and natural (bioinspired) computing.[1−3] Biocomputing is a novel branch in the unconventional computing area, relying upon the ability of biological systems to cope with and adapt to changing environmental conditions. Across many available biological organisms and systems (ant colony algorithms, neural cell networks, immune systems, genes, viruses), bacteria show great promise in biocomputing because of their unique combination of being a relatively simple organism with a complex genome that responds to and survives in a broad range of environmental conditions.[2,4,5] Recent studies have shown that bacteria are capable of sensing a wide range of stimuli and provide chemical and physical responses.[5−7] These properties open paths for bacteria to be employed in information storage platforms. For example, there are reports on the potential use of certain strains of bacteria as memory devices, logic networks and gates, genetic transistors (biological analog of semiconductor transistors), genetic circuits, as well as programmable biocomputational devices.[1,2,8] In addition, certain bacteria have been utilized as biosensors, represented as interfaces responding to certain types of input signals or conditions.[5,9] All the abovementioned factors and approaches make bacteria a perfect candidate for use in nonconventional biological computing systems or, to be more particular, create a separate direction of research—bacterial computing. Furthermore, the search for concepts of bacterial computing systems that can be used in certain areas with specific or extreme conditions requires studying the surface interactions of bacteria with technologically relevant inorganic materials in response to specific stimuli. Thus, gained knowledge and developed approaches can be applied to novel bioelectronic interfaces.

Pseudomonas aeruginosa is a biosafety level 2 (BSL-2) bacteria, a typical representative of in-hospital infections targeting people with a depressed immune system. *P. aeruginosa* becomes problematic for antimicrobial treatment because of its inherent resistance to many antibiotics, capability to rapidly acquire strong resistance to adverse external conditions, and ability to develop drug resistance using diverse mutations mechanisms.[10−13] It has been reported that *P. aeruginosa* is capable of forming tough and resilient biofilms on various substrates.[6,14,15] Furthermore, by transitioning from planktonic to biofilm form, *P. aeruginosa* significantly increases its survivability.[16,17] As Gram-negative bacteria, *P. aeruginosa* possesses adhesive pili that are involved in cell adhesion processes, biofilm formation, and bacteriophage adsorption.[18,19] All these specific properties related to its ability to survive and adapt to variable specific environments make *P. aeruginosa* a perfect candidate for potential use in biological computing where stability of the system under aggressive external conditions is one of the desired properties. Development of biointerfaces with stable and predictable intrinsic properties requires understanding the mechanisms of their formation along with parameters that can be affected by external stimuli. Recent studies discuss *P. aeruginosa* biofilms

Received: June 19, 2018
Revised: August 7, 2018
Published: August 19, 2018

DOI: 10.1021/acs.langmuir.8b02079
Langmuir 2018, 34, 10806−10815

and their attributes on certain substrates. However, there is a lack of fundamental knowledge to systematically characterize the formed biofilms on various substrates relevant to electronics application, particularly under different conditions.

In this study, we compare films of *P. aeruginosa* formed on Au, GaN, and SiO_x surfaces. Chemical and topographical parameters of the inorganic materials, known to be affecting the nucleation of biofilms, were investigated. Bacterial films were formed on the inorganic surfaces before and after the material (not the bacteria) was exposed to UV light (365 nm wavelength). We report on the antimicrobial capabilities, hydrophobicity, and change of chemical composition of the surface before and after UV light illumination. The properties of the biofilms and surfaces are compared using X-ray photoelectron spectroscopy (XPS) and atomic force microscopy (AFM). Calcium assay tests are utilized to estimate the effect of surface type on the change in cell membrane potential. The detailed characterization develops further understanding of the influence of substrate properties on the behavior of *P. aeruginosa* biofilms and potential for usage in robust bioelectronic platforms experiencing rapid change of external conditions.

RESULTS AND DISCUSSION

Surface Characterization Prior to Bacterial Film Formation. We chose to utilize three different types of inorganic substrates because they represent classes of materials often used in electronic interfaces. Numerous studies have used gold (Au) films as a model substrate to understand adsorption of biomolecules as well as cells.[20−22] Gold films provide inert, stable, and durable coating with impressive electric characteristics highly desirable in circuit electronics.[23,24] SiO_x is the second type of material we utilized because it is also heavily used in electronics. All modern metal oxide semiconductor field-effect transistors rely on a thick layer of oxide as insulation and passivation of the silicon surface providing an efficient electrical interface and thus making SiO_x one of the most technologically important inorganic materials. The third surface in our studies was GaN. We chose this wide band-gap semiconducting material because it is widely used in optoelectronics.[25−27] Previously published work examined the surface chemistry change caused by external stimuli,[28,29] but it will be beneficial to investigate approaches of noninvasive methods for the change in electronic properties. In addition, recent research has identified GaN as a material with great promise to be used in bioelectronics because of its stability in water and its biocompatibility characteristics in vitro and in vivo.[30,31]

Prior to bacterial film formation, we assessed differences in surface quality and topography. Figure 1 represents the surface roughness data comparison derived from AFM scans of the three types of clean material. The mean roughness values for SiO_x and for GaN were 0.533 ± 0.264 and 0.576 ± 0.379 nm, respectively. The data allow us to define SiO_x and GaN samples as flat surfaces without significant roughness fluctuations.[32−34] The root mean square (RMS) value for Au is relatively higher, 1.490 ± 1.268 nm. The bigger standard deviation in the values can be rationalized by the presence of distinct grains on the gold surface as a result of the thermal evaporation and has been discussed in the literature.[35−37] Overall, all surfaces used in the study did not show any specific topographic features or variations[38,39] that can hinder or enhance biomolecular adsorption or bacterial adhesion.

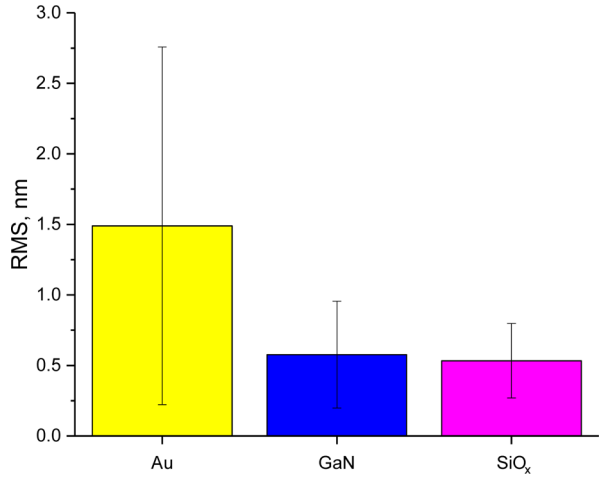

Figure 1. Mean roughness values for plane substrate surfaces of Au, GaN, and SiO_x.

We verified that the three different surfaces have no specific antibacterial activity. While many researchers are directing efforts to develop antibacterial surfaces, we seek to use a surface that does not kill bacteria. Thus, the chosen BSL-2 pathogenic bacteria biolayer regardless of its survivability properties should not be affected by the biocidal abilities of the substrate. Therefore, here, we want to identify a robust surface for use in bioelectronics that can be utilized as a predictable interface to trigger a bacterial response without destroying the biofilm. We performed a set of antibacterial tests to examine the Au, GaN, and SiO_x samples for potential biocidal properties. A method described in Foster et al.[40] was utilized to investigate the antibacterial behavior of the substrates. All three materials showed no significant differences compared with unmodified glass (negative control). Standard antibacterial tests involving the use of antibiotics were utilized as positive controls in these studies and helped to assess the survivability of *P. aeruginosa* on each type of material. Representative results seen on Figure 2 show that all tested

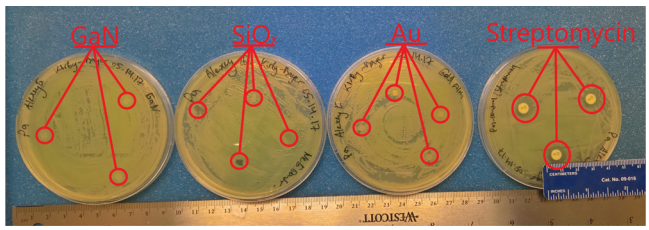

Figure 2. Representative digital pictures showing standard antibacterial tests of *P. aeruginosa* performed for Au, GaN, and SiO_x substrates. The positive control is represented by antimicrobial susceptibility disks with streptomycin.

materials exhibit no antibacterial behavior in a short-term (12 h) timeframe. We referenced the behavior of *P. aeruginosa* in contact with each of our materials to susceptibility disks with streptomycin, a widely used, broad spectrum antibiotic that targets protein synthesis and is used to target bacterial infections.[41] Reports in the literature have indicated that nanostructured surfaces and dissolved metal ions can lead to antibacterial effects.[7,15,42−44] In summary, the performed tests can confirm that all three surfaces are stable under the desired

DOI: 10.1021/acs.langmuir.8b02079
Langmuir 2018, 34, 10806−10815

biofilm formation conditions and do not degrade in any fashion that can harm the bacteria.

A critical component of a functional biointerface is its ability to trigger a response due to some type stimuli that is mediated by its chemical and/or electronic properties.[2,3,9] Rather than utilizing solution-based treatments, UV illumination of the samples was chosen as an environmental factor that can change surface properties and subsequently trigger an interfacial-mediated response associated with film formation. Sterilized wafer samples prepared accordingly were exposed to UV light prior to bacterial film formation. The reason for choosing a UV treatment is its simplicity, the fact that it does not require a specialized setup and it has been previously extensively studied as a disinfecting and cleaning treatment, and thus can be easily adapted to biointerfaces containing pathogenic organisms. Exposure to UV light of semiconductor materials results in charge accumulation on the surface, and reports in the literature have shown that the surface chemistry composition can be altered.[45−47] We assessed initial changes in surface properties by monitoring changes in the hydrophobicity/hydrophilicity of the substrates via contact angle measurements. The mean values for the contact angles on the Au, GaN, and SiO_x samples before and after exposure to UV light are summarized in Figure 3. All examined samples can be characterized as exhibiting hydrophobic behavior because their contact angles were consistently greater than 35−40°.[48] The mean value of the contact angle on Au was the highest at 63.34°, followed by 64.89° for GaN and 43.52° for SiO_x prior to UV light exposure. After UV light treatment of the samples, one can see small differences in the measured contact angles. The Au mean contact angle increased approximately by 5% and became 66.75°, whereas the GaN and SiO_x measurements decreased by 5% with values of 61.66° and 41.37°, respectively. On the basis of these observations, one can conclude that UV light exposure alone in air does not cause a statistically significant change in the hydrophobicity of any of the studied surfaces.

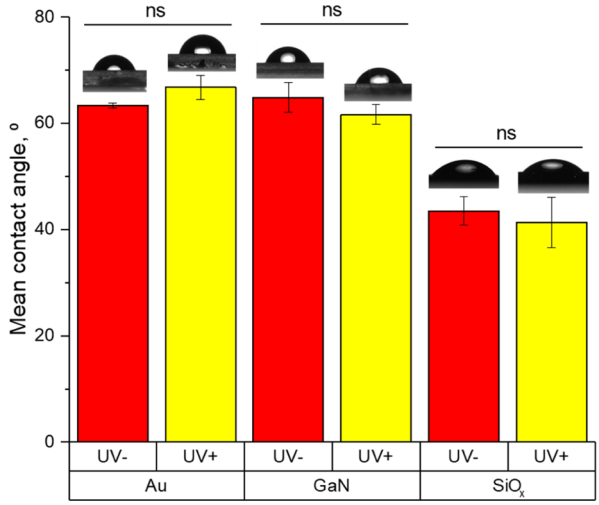

Figure 3. Mean contact angle values for Au, GaN and SiO_x materials before and after irradiation with UV light, ANOVA with $p < 0.05$. Representative digital pictures of water droplets on each sample are pasted above the bar graphs.

Quantitative surface characterization can provide further understanding of changes caused by UV irradiation of the samples. XPS is a widely utilized surface characterization tool for assessment of surface compositional changes.[49−54] Cleaned Au, GaN, and SiO_x samples were examined by XPS before exposing them to the UV light as well as after 1 h irradiation. Survey scans were collected and then analyzed to extract the surface chemical composition. Figure 4 summarizes the total composition changes in a bar graph format. Data are also compared in a table format in the Supporting Information. Here, we highlight the main observations with respect to the surface composition after exposure to UV light. On Au samples, compared to the clean, nonirradiated samples, the O concentration increased by 12.36%, the C concentration increased by 9.67%, and a small decrease by 3.93% was recorded in the amount of Au (Figure 4; Supporting Table 1). Upon statistical analysis, none of the changes observed on the Au samples before and after exposure to UV light can be considered significant. The same overall observation was made on GaN surfaces. The biggest change in the surface composition after exposure to UV light was recorded for O (55.68% increase from the original amount), followed by Ga which exhibited a 14.36% decrease. In addition, on the GaN surfaces, the C increased by 14.07% and N increased by 6.30%. Analysis of the data on SiO_x samples revealed the smallest compositional changes where the Si amount increased by 2.44%, the O decreased by 1.51%, and the C contribution decreased by 10.11%. Overall, the initial compositional changes supported the notion that further analysis of the high-resolution data is needed to understand specific surface transformations.

Many studies have reported UV light as an effective treatment for the removal of organic contaminants from the surface of various materials.[45,47,55] Furthermore, UV can be used to oxidize surfaces.[46,56] Therefore, we fitted and analyzed

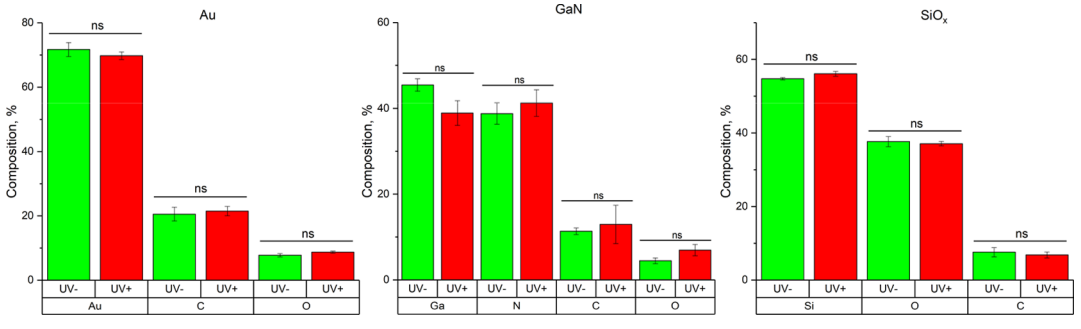

Figure 4. Mean values representing the chemical composition on the Au, GaN and SiO_x films before and after irradiation with UV light. XPS survey scans are averaged and statistically (ANOVA with $p < 0.05$) evaluated in OriginPro 2017.

DOI: 10.1021/acs.langmuir.8b02079
Langmuir 2018, 34, 10806−10815

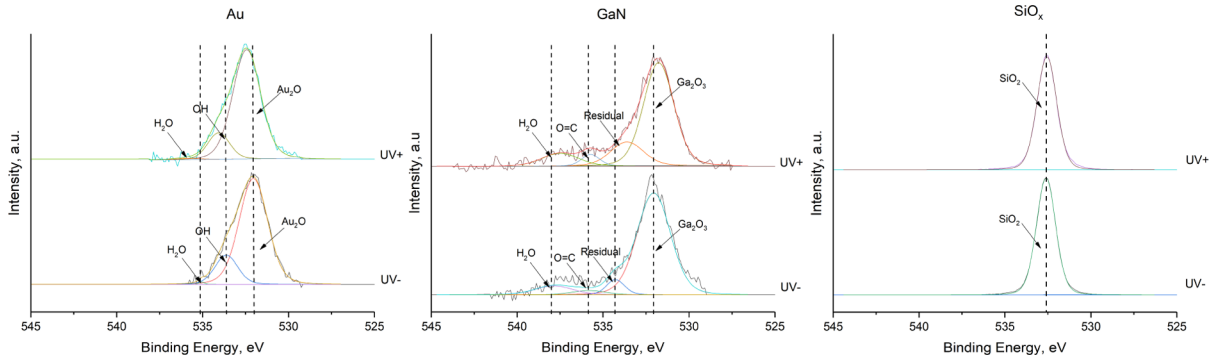

Figure 5. High resolution XPS scans of O 1s region on Au, GaN and SiO_x before and after irradiation with UV light. The dotted lines represent the location of important components identified after the data was analyzed by CasaXPS.

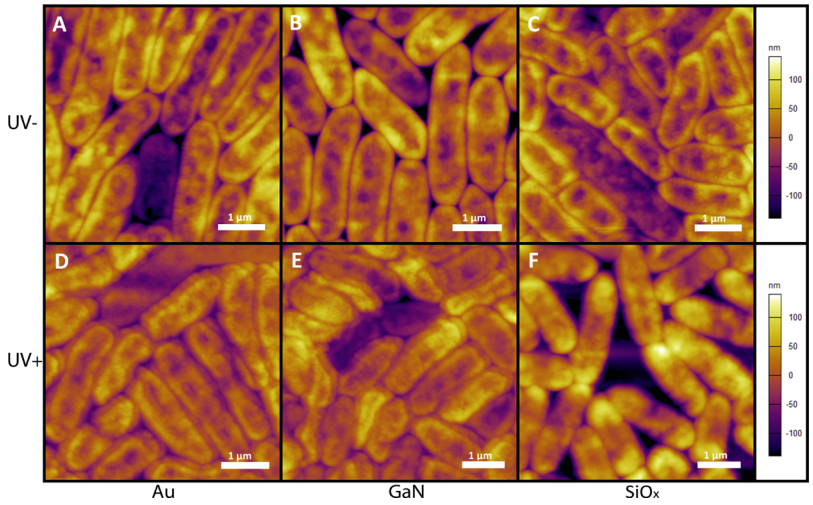

Figure 6. Representative AFM scans of *P. aeruginosa* films formed on materials not irradiated with UV light: (A) Au, (B) GaN and (C) SiO_x. The second row shows (D) Au, (E) GaN and (F) SiO_x samples with biofilms formed when the surfaces were treated with UV light for 1 h prior to exposure to bacteria.

the O 1s spectra collected on all of our samples. Figure 5 compares changes on each type of material before and after UV exposure and identifies major species after the data were fitted by CasaXPS. Additional analysis is presented in a table format in the Supporting Information section. On Au samples, the spectra are asymmetrical with a tail extending toward higher binding energy, which is consistent with previous research results.[52] Upon deconvoluting of the data using established parameters available in the literature,[51,52,54] the following species were assigned: O^{2-} (Au_2O) at 531.94 eV contributing to 81.09% of the total O composition and OH at 533.33 eV comprising 18.14% and H_2O at 534.68 eV responsible for 0.77%. After UV light exposure, we analyzed the data and assigned the following species: O^{2-} (Au_2O) peak was found at 532.11 eV, OH at 533.73 eV, and the H_2O peak at 535.50 eV. After UV light treatment, the OH species concentration decreased by 10.07%, O^{2-} (Au_2O) increased by 2.74%, and the most significant change was in the amount of water−H_2O contribution which decreased by 33.77%. GaN nonirradiated samples have four main species[51] in the O 1s spectrum: O^{2-} (as in Ga_2O_3) at 532.05 eV, residual-OH Ga at 534.28 eV, O═C at 535.81 eV, and H_2O at 537.86 eV. Upon exposure to the UV light, we recorded the following components: 531.70 eV for O^{2-} (as in Ga_2O_3), residual-OH Ga peak at 533.56 eV, O═C contribution at 535.68 eV, and H_2O peak at 537.44 eV. A significant change in all component contributions was observed (see the Supporting Information), with the largest for residual-OH Ga with 161% increase, whereas the O═C species increased by 38.94%, the H_2O contribution increased by 28.74%, and the O^{2-} (as in Ga_2O_3) peak reduced by 17.05%. Analysis of the O 1s spectra on thermally grown SiO_x revealed one sharp peak, which remained symmetrical before and after UV exposure and centered at 532.61 and 532.66 eV, respectively. Taken in sum, the XPS data indicate that there is significant change in the types of oxide species present on the surface of the UV-treated samples of Au and GaN. This is an important observation to consider in order to rationalize the results presented further in the study.

***P. aeruginosa* Film Characterization.** The morphological and adhesion properties of the *P. aeruginosa* films formed on Au, GaN, and SiO_x surfaces were characterized by AFM. Many researchers have utilized AFM as one of the main tools for gaining structural and functional data under different conditions[57−63] along with studying membrane protein localization and molecular interactions.[64−67] Figure 6 shows representative topographical images of the films formed on Au, GaN, and SiO_x samples before and after exposure to the UV light. Overall, the biofilms are densely packed, and the *P. aeruginosa* cells appear healthy and express no evidence of chemical rupture, physical disturbance, or any membrane damage signs. The AFM scans were analyzed to extract the

DOI: 10.1021/acs.langmuir.8b02079
Langmuir 2018, 34, 10806−10815

length-to-width ratio, which is one of important parameters related to the bacteria growth. For statistical analysis, at least three samples of each material under each condition were utilized. Up to 10−12 cells were measured on each AFM scan. Figure 7 compares the mean length-to-width ratios for Au, GaN, and SiO_x samples before and after exposing to the UV light. We recorded significant differences in the mean ratios of films grown on samples that were either exposed or not exposed to UV light in the cases of Au and GaN. The ratio for films on Au decreased by 13% (from 3.0 to 2.6), and for films on GaN, the decrease was equal to 24% (from 3.4 to 2.6). An opposite trend was observed for films grown on SiO_x samples exposed to UV light or not prior to *P. aeruginosa* introduction. The mean length-to-width ratio had a nonsignificant increase by 8% (from 2.5 to 2.7).

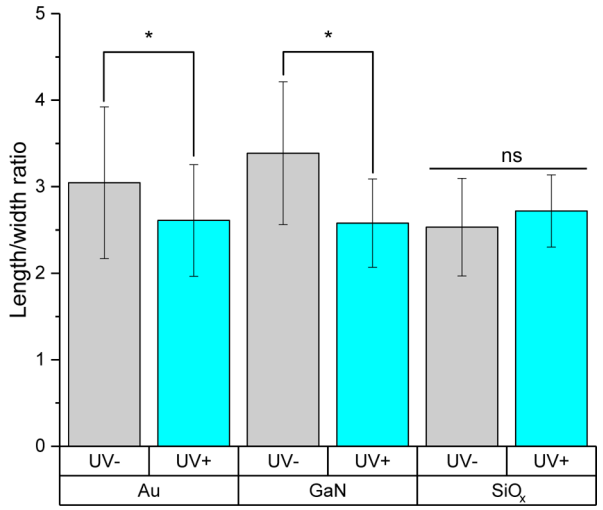

Figure 7. Mean length-to-width ratios of *P. aeruginosa* cells formed on Au, GaN and SiO_x surfaces before and after irradiation with UV light. The averaged data extracted from AFM scans was statistically (ANOVA with $p < 0.05$) analyzed in OriginPro 2017.

Additionally, we utilized the AFM data to assess changes to the cell wall organization, specifically the generation of outer membrane vesicles (OMV) by quantifying changes on an individual cell surface roughness. OMV are components of the bacteria stress response which aid in nutrient procurement, biofilm production, and pathogenicity.[68] Bacteria generating OMV, also called blebbing, have a roughened cell surface. An individual cell RMS value was extracted by drawing a line along the bacteria center of symmetry along the entire cell. In a similar manner to the analysis described above, at least three samples in three different regions were scanned on each substrate as well as under each UV light condition. Up to 10−12 cells were measured from each AFM scan. Figure 8 compares all the data extracted from this analysis. When one compares the data on each material where films were formed on surfaces that were either treated by UV light or not, statistically, there were no significant differences when the data are analyzed for differences on each material after treatment. However, it is important to note that the mean RMS values on Au and GaN decreased on materials treated by UV light, but the opposite behavior was observed on SiO_x. In general, the morphological analysis performed by AFM supports the notion that the nature of the material and UV light treatment can change the properties of the *P. aeruginosa* cells comprising the films on the surface.

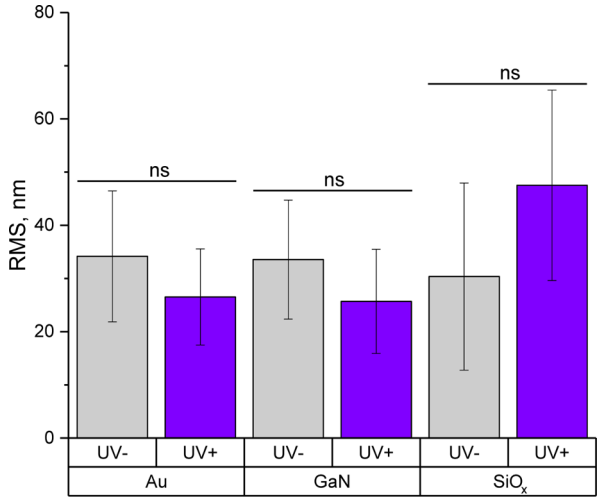

Figure 8. "Blebbing effect" caused by UV treatment. Mean roughness values of single *P. aeruginosa* cells scanned with AFM on Au, GaN and SiO_x surfaces before and after irradiation with UV light. The extracted values were averaged and statistically (ANOVA with $p < 0.05$) evaluated in OriginPro 2017.

Biofilm adhesion is a property that is important to assess because it is closely connected to film growth and development.[18,69−74] Further AFM characterization of the *P. aeruginosa* films was done by force volume maps. A representative map along with a histogram extracted from it is shown on Figure 9A. The force volume scan was done as a 32 × 32 point image, and each force volume map was used to extract a mean adhesion force value. For statistical comparisons, a minimum of three force maps for each substrate and each condition were collected. The data were analyzed in both the Asylum Research software package and OriginPro utilizing 2-way analysis of variance (ANOVA). In Figure 9B, a statistical comparison for the films on Au, GaN, and SiO_x samples before and after UV light irradiation is presented. The data show a visible change in adhesion force for all samples before and after UV light exposure. However, the change of adhesion force on GaN samples, which experienced 61% decrease, was statistically significant. Additionally, on Au surfaces, there was a 48% decrease in adhesion force, and an opposite trend was recorded for SiO_x surfaces with a 64% increase in adhesion force on films grown on material after UV light irradiation. The adhesion data correlate with the morphological data described in the previous section as well as with the data extracted by surface characterization. Thus, changes in surface chemistry (residual OH and O^{2-}) caused by UV irradiation affect the biofilm properties. At the same time, certain other properties, such as substrate hydrophobicity can have a negligible effect on biofilm formation, which correlates with conclusions from prior literature.[71,75−77]

Recent research defines Ca^{2+} as an important indicator and a regulative factor in a wide range of biological systems. Both intracellular and intercellular Ca^{2+} concentrations define and influence numerous functions in eukaryotic and prokaryotic cells.[78,79] For example, in eukaryotes, Ca^{2+} serves as an universal transmitter of signals from the surface to the cell core.[80] Apart from that, in prokaryotes, free Ca^{2+} is known to play a role in physiological processes, such as spore formation, virulence, and change in cell differentiation.[81] Free intercellular

DOI: 10.1021/acs.langmuir.8b02079
Langmuir 2018, 34, 10806−10815

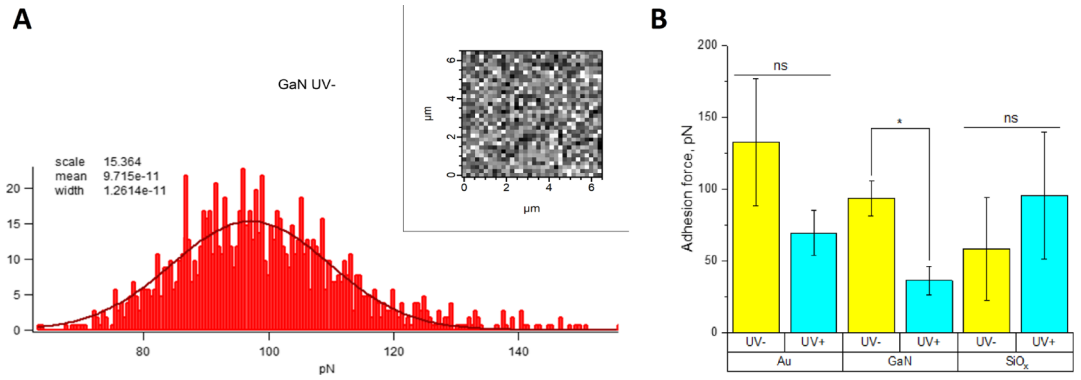

Figure 9. (A) Surface adhesion histogram obtained from AFM adhesion force map (seen in the inset). Both figures represent data for *P. aeruginosa* biofilm on the surface of GaN substrate before UV light irradiation. (B) Mean surface adhesion values of *P. aeruginosa* biofilms on Au, GaN and SiO_x samples before and after UV light treatment. Adhesion force histograms were averaged and statistically (ANOVA with $p < 0.05$) evaluated in OriginPro 2017.

Ca^{2+} is associated with regulation of cell processes involving structural integrity, motility, metabolism, life cycle, pathogenesis, sporulation, transport, and stress signals.[80] Possible changes in intercellular Ca^{2+} gradients can be viewed as an internal physiological response of bacteria cells to changes in environmental conditions,[82−84] and it is therefore an important parameter to consider when analyzing the properties of the formed *P. aeruginosa* films and morphological responses to the substrate materials we studied.

The quantification of intracellular Ca^{2+} concentrations is done by assays utilizing different readouts based on optical changes such as photoluminescence and fluorescence.[44,79] We utilized a Fluo-4 Direct Calcium Assay that is based on a fluorescence signal and has been tested on various types of biological systems.[44,85] Multiple time points were scanned and two points showing the response of the stabilized solution under ambient conditions were extracted and analyzed in OriginPro. The summarized data for 20 and 30 min time points on all materials under different conditions are shown in Figure 10. Statistical analysis clearly shows a difference between films grown on samples before and after UV illumination. Variations in Ca^{2+} concentrations are typically linked to changes in the integrity of the cell wall, but it can also be indicative of other biological factor alterations.[80,81] With respect to our study, the Fluo-4 Direct Calcium Assay support the notion that the altered surface properties after UV exposure facilitate the formation of biofilms with different mechanical properties.

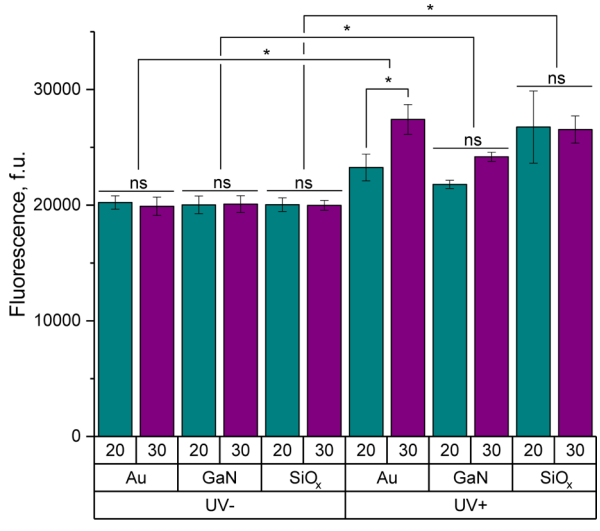

Figure 10. Summary of Fluo-4 Direct Calcium Assay results. Fluorescence measurements were taken after 20 and 30 min for *P. aeruginosa* cells grown on the Au, GaN and SiO_x substrates before and after UV light treatment. The data was averaged and statistically (ANOVA with $p < 0.05$) evaluated in OriginPro 2017.

CONCLUSIONS

In summary, we recorded and analyzed the *P. aeruginosa* biofilm formation mechanism on the surface of Au, GaN, and SiO_x under different environmental conditions by exposing the materials to UV light prior to film formation. The surface chemistry does change upon exposure to the UV, and in turn can induce the differences in the biofilm properties. The wide band gap semiconductor material, GaN, is more versatile substrate for biocomputing applications and is the only one that shows noteworthy effects because that is where one would expect all the surface states (and its persistent photoconductivity) to be significant. Specifically, individual bacteria within films can differ in their morphological characteristics as well as adhesion characteristics. Furthermore, films grown on surfaces after exposure to UV light uniformly show higher intracellular Ca^{2+} concentrations consistent with a different mechanical response. The results of this work can be used to design functional interfaces that utilize both the properties of the material as well as morphological and biological change in the bacterial biofilm.

EXPERIMENTAL SECTION

Materials and Supplies. All commercial materials and supplies were used as received according to the manufacturer's instructions: *P. aeruginosa* (Schroeter) Migula (ATCC 27853) was obtained from ATCC; tryptic soy broth, prepared media bottle, 125 mL (item # 776840), was obtained from Carolina Biological Supply Company; Thermo Scientific nutrient soy agar powder, 500 g (Cat. CM0003B); Fisherbrand Petri dishes with a clear lid (Cat. FB0875714); Oxoid streptomycin/penicillin/novobiocin antimicrobial susceptibility disks (Cat. CT0047B; Cat. CT1755B) were obtained from Thermo Fisher Scientific; Invitrogen Fluo-4 Direct Calcium Assay Kit (Cat. F10471) was obtained from Thermo Fisher Scientific; High Quality (HQ) HQ-75-Au AFM Probes with frequency f = 75 kHz and spring constant k = 2.5 N/m were obtained from Oxford Instruments. Ga-polar GaN was grown as previously reported.[86] Semitransparent Au thin films (20 nm thickness) were deposited by e-beam on ∼1.3 μm

DOI: 10.1021/acs.langmuir.8b02079
Langmuir 2018, 34, 10806−10815

thick Ga-polar (0001) GaN on a 430 μm thick Al_2O_3 substrate with a 5 nm of Ti adhesion layer. SiO_x wafers were purchased from University Wafer with 500 nm thermally grown oxide.

Wafer Sample Preparation. All wafer samples for every test performed in this study were prepared in the same way to maintain sterility of samples. Wafer samples were sterilized by autoclaving at 121 °C for 30 min and then stored for 3 days to equilibrate a possible effect of autoclaving on the material surface.

Biofilm Sample Preparation. Tryptic soy broth was autoclaved at 121 °C for 25 min and then slowly cooled to room temperature. A *P. aeruginosa* (*P.a.*) dry pellet was dissolved in 20 mL sterile tryptic soy broth, vortexed for 120 s, and then placed in the shaking incubator (environmental shaker) at 37 °C to incubate overnight. The rest of the *P.a.* dry pellet was frozen using 15% glycerol solution according to standard freezing protocols and stored at −78 °C. Tryptic soy agar plates were prepared for further use where 16 g of nutrient soy agar powder was dissolved in 400 mL of deionized (DI) water. Subsequently, the solution was autoclaved at 121 °C for 25 min and slowly cooled to room temperature. The solution was poured into Petri dishes and after overnight cooling was available for further use. Using a method adapted from Foster et al.,[40] we transferred 5 mL of bacterial suspension washed by vortexing for 60 s 3 times in 10 mL of sterile DI water and then centrifuged at 5000*g* for 10 min. The pellet that was obtained was suspended in 500× tryptic soy broth to obtain a solution of approximately 2×10^8 CFU/mL, as required by the adapted protocol. The concentration was confirmed with a BioMate3 spectrophotometer (Thermo Electron Corporation) at o.d. 600 nm. A droplet (approximately 10 μL) of the obtained solution was transferred to tryptic soy agar plates and spread across the area of the Petri dish with a sterile culture spreader. Sterile wafer pieces from the test materials (GaN, Au, or SiO_x) were put face down onto the agar. The samples were incubated at 37 °C for 8 h to obtain a biofilm of desired density. The samples designated as UV+ were produced the same way; however, prior to the biofilm preparation, the inorganic surfaces were exposed to UV lamp illumination for 1 h. [Longwave UV Lamps (Analytik Jena) with a 365 nm wavelength].

Antibacterial Tests. Adapted from Foster et al.,[40] the method includes a preparation of a "sandwich": a wafer piece of a test material is placed on a sterile coverslip, and a droplet of bacterial suspension is put on the top of wafer sample and then covered with a round coverslip. The prepared "sandwich" is transferred into a Petri dish on gauze moistened with water and then incubated at 37 °C for 1, 4, 12, and 24 h. After the incubation, the entire "sandwich" is placed in 20 mL of sterile DI water and vortexed for 60 s. This suspension is used to make 1:10−1:1000 dilutions in DI water. Subsequently, even droplets of desired concentrations are transferred and spread in a fresh nutrient agar plate. Prepared plates were incubated as directed and used for further data analysis. The adapted Kirby−Bauer technique[87] requires 4−5 individual colonies picked from the agar plate be transferred to 5 mL of sterile DI water. The suspension was vortexed for 60 s. A fresh nutrient agar plate was inoculated evenly with an inoculation loop. Sterile samples were put face down, and antimicrobial susceptibility disks with various antibiotics were also transferred. Prepared samples were incubated at 37 °C overnight, and representative digital photos of grown cultures were taken with a Nikon D3300 camera.

Calcium Assay Test. Prepared UV− and UV+ samples were washed in 5 mL of sterile DI water at 5000*g* for 5 min. The cell concentration was checked with a BioMate3 spectrophotometer and showed comparable results for samples composed of different materials. Utilizing the manufacturer's protocol, prepared Fluo-4 Direct Calcium Assay was added to 24-well plates with cell suspensions and then incubated in the dark at 37 °C for 1 h. Fluorescence measurements were performed using a Tecan GENios microplate reader with 485 nm excitation and 535 nm emission filters installed. Analysis of the obtained data was done using OriginPro 2017 (v. 9.4.1.354).

AFM Characterization. Asylum Research Cypher was utilized to obtain at least three scans of random areas of prepared film samples and clean materials. HQ-75-Au AFM cantilevers with frequency f = 75 kHz, and spring constant k = 2.5 N/m were used at a scanning frequency of 0.5 Hz to obtain images of 5 × 5 μm areas. The tapping mode was performed in air at room temperature. Force maps were generated for biofilm samples using the same cantilevers. Generated images and adhesion force maps were processed using Asylum Research software (v. 13.01.68) bundled into Igor Pro (v. 6.22). RMS roughness and adhesion force values were extracted for comparison among all samples. Cell geometrical parameters were obtained from AFM scans using ImageJ software package (v. 1.51q).

XPS Characterization. All data were collected with Kratos Analytical Axis Ultra XPS. Wide survey scans were acquired with 160 eV pass energy. High-resolution data were collected for the following: Au 4f, Ga 3d, Ga 2p, Si 2p, C 1s, N 1s, O 1s, and S 2p at a pass energy of 20 eV. Atomic compositions of elements and peak fits were analyzed using CasaXPS software package (v. 2.3.19). Peak calibrations were performed by setting the adventitious C 1s peak to be equal to 284.8 eV.

Contact Angle. Contact angle measurements were recorded on a ramé-hart automated dispensing system, and 1.2 μL of DI water droplets was deposited onto Au, GaN, and SiO_x wafer samples. The ramé-hart model 200 F4 series standard goniometer was used to collect images. OnScreenProtractor Java-applet (v. 0.5) was employed to analyze the droplet images.

Statistical Analysis. Data analysis was carried out using one-way, two-way, and three-way ANOVA methods with OriginPro 2017 (v. 9.4.1.354).

■ ASSOCIATED CONTENT

Supporting Information

The Supporting Information is available free of charge on the ACS Publications website at DOI: 10.1021/acs.langmuir.8b02079.

Additional experimental details, statistical analysis, and characterization data (PPTX)

■ AUTHOR INFORMATION

Corresponding Author

*E-mail: ivanisevic@ncsu.edu.

ORCID

Dennis R. LaJeunesse: 0000-0001-5049-8968

Albena Ivanisevic: 0000-0003-0336-1170

Notes

The authors declare no competing financial interest.

■ ACKNOWLEDGMENTS

We thank Army Research Office under W911NF-15-1-0375 for support of this work. Partial financial support from NSF (DMR-1312582 and ECCS-1653383) is greatly appreciated.

■ REFERENCES

(1) Katz, E. Biocomputing - Tools, Aims, Perspectives. *Curr. Opin. Biotechnol.* **2015**, *34*, 202−208.

(2) Simpson, M. L.; Sayler, G. S.; Fleming, J. T.; Applegate, B. Whole-Cell Biocomputing. *Trends Biotechnol.* **2001**, *19*, 317−323.

(3) Bedbrook, C. N.; Yang, K. K.; Rice, A. J.; Gradinaru, V.; Arnold, F. H. Machine Learning to Design Integral Membrane Channelrhodopsins for Efficient Eukaryotic Expression and Plasma Membrane Localization. *PLoS Comput. Biol.* **2017**, *13*, No. e1005786.

(4) Bradley, R. W.; Buck, M.; Wang, B. Tools and Principles for Microbial Gene Circuit Engineering. *J. Mol. Biol.* **2016**, *428*, 862−888.

(5) Amos, M.; Axmann, I. M.; Blüthgen, N.; de la Cruz, F.; Jaramillo, A.; Rodriguez-Paton, A.; Simmel, F. Bacterial Computing with Engineered Populations. *Philos. Trans. R. Soc., A* **2015**, *373*, 20140218.

(6) Zhang, J.; Huang, J.; Say, C.; Dorit, R. L.; Queeney, K. T. Deconvoluting the Effects of Surface Chemistry and Nanoscale

DOI: 10.1021/acs.langmuir.8b02079
Langmuir 2018, 34, 10806−10815

Topography: Pseudomonas Aeruginosa Biofilm Nucleation on Si-Based Substrates. *J. Colloid Interface Sci.* **2018**, *519*, 203−213.
(7) Ramalingam, B.; Parandhaman, T.; Das, S. K. Antibacterial Effects of Biosynthesized Silver Nanoparticles on Surface Ultrastructure and Nanomechanical Properties of Gram-Negative Bacteria Viz. Escherichia Coli and Pseudomonas Aeruginosa. *ACS Appl. Mater. Interfaces* **2016**, *8*, 4963−4976.
(8) Purcell, O.; Lu, T. K. Synthetic Analog and Digital Circuits for Cellular Computation and Memory. *Curr. Opin. Biotechnol.* **2014**, *29*, 146−155.
(9) Lahoz-Beltra, R.; Navarro, J.; Marijuán, P. C. Bacterial Computing: A Form of Natural Computing and Its Applications. *Front. Microbiol.* **2014**, *5*, 101.
(10) Rolsma, S.; Frank, D. W.; Barbieri, J. T.; Rolsma, S.; Frank, D. W.; Barbieri, J. T. Pseudomonas Aeruginosa Toxins. *The Comprehensive Sourcebook of Bacterial Protein Toxins*; Elsevier, 2015; pp 133−160.
(11) Wu, W.; Jin, Y.; Bai, F.; Jin, S. Pseudomonas Aeruginosa. *Molecular Medical Microbiology*; Elsevier, 2015; pp 753−767.
(12) Yayan, J.; Ghebremedhin, B.; Rasche, K. No Outbreak of Vancomycin and Linezolid Resistance in Staphylococcal Pneumonia over a 10-Year Period. *PLoS One* **2015**, *10*, No. e0138895.
(13) Hancock, R. E. W. Resistance Mechanisms inPseudomonas aeruginosaand Other Nonfermentative Gram-Negative Bacteria. *Clin. Infect. Dis.* **1998**, *27*, S93−S99.
(14) Mitik-Dineva, N.; Wang, J.; Truong, V. K.; Stoddart, P.; Malherbe, F.; Crawford, R. J.; Ivanova, E. P. Escherichia Coli, Pseudomonas Aeruginosa, and Staphylococcus Aureus Attachment Patterns on Glass Surfaces with Nanoscale Roughness. *Curr. Microbiol.* **2009**, *58*, 268−273.
(15) Amézaga-Madrid, P.; Silveyra-Morales, R.; Córdoba-Fierro, L.; Nevarez-Moorillon, G.; Miki-Yoshida, M.; Orrantia-Borunda, E. TEM Evidence of Ultrastructural Alteration on Pseudomonas Aeruginosa by Photocatalytic TiO2 Thin Films. *J. Photochem. Photobiol., B* **2003**, *70*, 45−50.
(16) Sauer, K.; Camper, A. K.; Ehrlich, G. D.; Costerton, J. W.; Davies, D. G. Pseudomonas Aeruginosa Displays Multiple Phenotypes during Development as a Biofilm. *J. Bacteriol.* **2002**, *184*, 1140−1154.
(17) Caiazza, N. C.; Merritt, J. H.; Brothers, K. M.; O'Toole, G. A. Inverse Regulation of Biofilm Formation and Swarming Motility by Pseudomonas Aeruginosa PA14. *J. Bacteriol.* **2007**, *189*, 3603−3612.
(18) Touhami, A.; Jericho, M. H.; Boyd, J. M.; Beveridge, T. J. Nanoscale Characterization and Determination of Adhesion Forces of Pseudomonas Aeruginosa Pili by Using Atomic Force Microscopy. *J. Bacteriol.* **2006**, *188*, 370−377.
(19) Kuchma, S. L.; O'Toole, G. A. Surface-Induced and Biofilm-Induced Changes in Gene Expression. *Curr. Opin. Biotechnol.* **2000**, *11*, 429−433.
(20) Kashefi-Kheyrabadi, L.; Noori, A.; Mehrgardi, M. A. Application of Bioconjugated Nanoporous Gold Films in Electrochemical Biosensors. *Biosensors Nanotechnology*; Wiley, 2014.
(21) Gupta, G.; Rajendran, V.; Atanassov, P. Laccase Biosensor on Monolayer-Modified Gold Electrode. *Electroanalysis* **2003**, *15*, 1577−1583.
(22) López-Muñoz, G. A.; Estévez, M.-C.; Vázquez-García, M.; Berenguel Alonso, M.; Alonso-Chamarro, J.; Homs-Corbera, A.; Lechuga, L. M. Gold/Silver/Gold Trilayer Films On Nanostructured Polycarbonate Substrates For Direct And Label-Free Nanoplasmonic Biosensing. *J. Biophot.* **2018**, *11*, No. e201800043.
(23) Roberts, G. *Van Nostrand's Scientific Encyclopedia*, 2005.
(24) Vilan, A.; Yaffe, O.; Biller, A.; Salomon, A.; Kahn, A.; Cahen, D. Molecules on Si: Electronics with Chemistry. *Adv. Mater.* **2010**, *22*, 140−159.
(25) Lidow, A.; Strydom, J.; de Rooij, M.; Reusch, D. GaN Transistors for Efficient Power Conversion—Application Examples. *GaN Transistors for Efficient Power Conversion*; Wiley, 2014; p 266.
(26) Jia, H.; Guo, L.; Wang, W.; Chen, H. Recent Progress in GaN-Based Light-Emitting Diodes. *Adv. Mater.* **2009**, *21*, 4641−4646.
(27) Garrett, G. A.; Rotella, P.; Shen, H.; Wraback, M.; Haeger, D. A.; Chung, R. B.; Pfaff, N.; Young, E. C.; DenBaars, S. P.; Speck, J. S.; et al. Carrier Dynamics in Active Regions for Ultraviolet Optoelectronics Grown on Thick, Relaxed AlGaN on Semipolar Bulk GaN. *Phys. Status Solidi B* **2012**, *249*, 507−510.
(28) Bain, L. E.; Kirste, R.; Johnson, C. A.; Ghashghaei, H. T.; Collazo, R.; Ivanisevic, A. Neurotypic Cell Attachment and Growth on III-Nitride Lateral Polarity Structures. *Mater. Sci. Eng., C* **2016**, *58*, 1194−1198.
(29) Snyder, P. J.; Kirste, R.; Collazo, R.; Ivanisevic, A. Nanoscale Topography, Semiconductor Polarity and Surface Functionalization: Additive and Cooperative Effects on PC12 Cell Behavior. *RSC Adv.* **2016**, *6*, 97873−97881.
(30) Lee, H. E.; Choi, J.; Lee, S.-H.; Jeong, M.; Ho Shin, J.; Joe, D.; Kim, D.; Wan Kim, C.; Park, J. H.; Hee Lee, J.; et al. Monolithic Flexible Vertical GaN Light-Emitting Diodes for a Transparent Wireless Brain Optical Stimulator. *Adv Mater.* **2018**, *30*, No. e1800649.
(31) Templier, F. GaN-Based Emissive Microdisplays: A Very Promising Technology for Compact, Ultra-High Brightness Display Systems. *J. Soc. Inf. Disp.* **2016**, *24*, 669−675.
(32) Curiel, M. A.; Nedev, N.; Nesheva, D.; Soares, J.; Haasch, R.; Sardela, M.; Valdez, B.; Sankaran, B.; Manolov, E.; Bineva, I.; et al. Microstructural Characterization of Thin SiOx Films Obtained by Physical Vapor Deposition. *Mater. Sci. Eng., B* **2010**, *174*, 132−136.
(33) Youtsey, C.; Adesida, I.; Romano, L. T.; Bulman, G. Smooth N-Type GaN Surfaces by Photoenhanced Wet Etching. *Appl. Phys. Lett.* **1998**, *72*, 560−562.
(34) Collazo, R.; Mita, S.; Aleksov, A.; Schlesser, R.; Sitar, Z. Growth of Ga- and N- Polar Gallium Nitride Layers by Metalorganic Vapor Phase Epitaxy on Sapphire Wafers. *J. Cryst. Growth* **2006**, *287*, 586−590.
(35) Oliva, A. I.; Anguiano, E.; Sacedón, J. L.; Aguilar, M.; Méndez, J. A.; Aznárez, J. A. Extended Statistical Analysis of Rough Growth Fronts in Gold Films Prepared by Thermal Evaporation. *Phys. Rev. B: Condens. Matter Mater. Phys.* **1999**, *60*, 2720−2727.
(36) Hoffmann, H.; Vancea, J. Critical Assessment of Thickness-Dependent Conductivity of Thin Metal Films. *Thin Solid Films* **1981**, *85*, 147−167.
(37) Aguilar, M.; Oliva, A. I.; Quintana, P.; Peña, J. L. Dynamic Phenomena in the Surface of Gold Thin Films: Macroscopic Surface Rearrangements. *Surf. Sci.* **1997**, *380*, 91−99.
(38) Boyd, R. D.; Verran, J.; Jones, M. V.; Bhakoo, M. Use of the Atomic Force Microscope to Determine the Effect of Substratum Surface Topography on Bacterial Adhesion. *Langmuir* **2002**, *18*, 2343−2346.
(39) Hsu, L. C.; Fang, J.; Borca-Tasciuc, D. A.; Worobo, R. W.; Moraru, C. I. Effect of Micro- and Nanoscale Topography on the Adhesion of Bacterial Cells to Solid Surfaces. *Appl. Environ. Microbiol.* **2013**, *79*, 2703−2712.
(40) Foster, H. A.; Sheel, D. W.; Sheel, P.; Evans, P.; Varghese, S.; Rutschke, N.; Yates, H. M. Antimicrobial Activity of Titania/Silver and Titania/Copper Films Prepared by CVD. *J. Photochem. Photobiol., A* **2010**, *216*, 283−289.
(41) Yayan, J.; Ghebremedhin, B.; Rasche, K. No Outbreak of Vancomycin and Linezolid Resistance in Staphylococcal Pneumonia over a 10-Year Period. *PLoS One* **2015**, *10*, No. e0138895.
(42) Lemire, J. A.; Harrison, J. J.; Turner, R. J. Antimicrobial Activity of Metals: Mechanisms, Molecular Targets and Applications. *Nat. Rev. Microbiol.* **2013**, *11*, 371−384.
(43) Nguyen, D. H. K.; Pham, V. T. H.; Truong, V. K.; Sbarski, I.; Wang, J.; Balčytis, A.; Juodkazis, S.; Mainwaring, D. E.; Crawford, R. J.; Ivanova, E. P. Role of Topological Scale in the Differential Fouling of Pseudomonas Aeruginosa and Staphylococcus Aureus Bacterial Cells on Wrinkled Gold-Coated Polystyrene Surfaces. *Nanoscale* **2018**, *10*, 5089−5096.
(44) Cao, H.; Qin, H.; Zhao, Y.; Jin, G.; Lu, T.; Meng, F.; Zhang, X.; Liu, X. Nano-Thick Calcium Oxide Armed Titanium: Boosts Bone

DOI: 10.1021/acs.langmuir.8b02079
Langmuir 2018, 34, 10806−10815

Cells against Methicillin-Resistant Staphylococcus Aureus. *Sci. Rep.* **2016**, *6*, 21761.
(45) Rudakowski, S. UV Light—A Powerful Tool for Surface Treatment. http://www.circuitnet.com; 2010, pp 1−6.
(46) Hook, D. A.; Olhausen, J. A.; Krim, J.; Dugger, M. T. Evaluation of Oxygen Plasma and UV Ozone Methods for Cleaning of Occluded Areas in MEMS Devices. *J. Microelectromech. Syst.* **2011**, *19*, 1292−1298.
(47) Cumpson, P.; Sano, N. Stability of Reference Masses V: UV/Ozone Treatment of Gold and Platinum Surfaces. *Metrologia* **2013**, *50*, 27−36.
(48) Smith, T. The Hydrophilic Nature of a Clean Gold Surface. *J. Colloid Interface Sci.* **1980**, *75*, 51−55.
(49) Domínguez-Crespo, M. A.; Brachetti-Sibaja, S. B.; Torres-Huerta, A. M.; De La Cruz-Hernández, W. Rare Earth Conversion Coatings Grown on AA6061 Aluminum Alloys. Corrosion Studies. *J. Mex. Chem. Soc.* **2014**, *58*, 393−410.
(50) Tracy, K. M.; Mecouch, W. J.; Davis, R. F.; Nemanich, R. J. Preparation and characterization of atomically clean, stoichiometric surfaces ofn- andp-type GaN(0001). *J. Appl. Phys.* **2003**, *94*, 3163−3172.
(51) Foster, C. M.; Collazo, R.; Sitar, Z.; Ivanisevic, A. Aqueous Stability of Ga- and N-Polar Gallium Nitride. *Langmuir* **2013**, *29*, 216−220.
(52) Kruse, N.; Chenakin, S. XPS Characterization of Au/TiO2 Catalysts: Binding Energy Assessment and Irradiation Effects. *Appl. Catal., A* **2011**, *391*, 367−376.
(53) Moulder, J. F. The Impact of the Scanning XPS Microprobe on Industrial Applications of X-Ray Photoelectron Spectroscopy. *J. Electron Spectrosc. Relat. Phenom.* **2018**, in press, DOI: 10.1016/j.elspec.2018.04.003
(54) Antunes, V. G.; Figueroa, C. A.; Alvarez, F. A Comprehensive Study of the TiN/Si Interface by X-Ray Photoelectron Spectroscopy. *Appl. Surf. Sci.* **2018**, *448*, 502−509.
(55) Moldovan, A.; Feldmann, F.; Krugel, G.; Zimmer, M.; Rentsch, J.; Hermle, M.; Roth-Fölsch, A.; Kaufmann, K.; Hagendorf, C. Simple Cleaning and Conditioning of Silicon Surfaces with UV/Ozone Sources. *Energy Procedia* **2014**, *55*, 834−844.
(56) King, D. E. Oxidation of gold by ultraviolet light and ozone at 25 °C. *J. Vac. Sci. Technol., A* **1995**, *13*, 1247−1253.
(57) Dufrêne, Y. F. Recent Progress in the Application of Atomic Force Microscopy Imaging and Force Spectroscopy to Microbiology. *Curr. Opin. Microbiol.* **2003**, *6*, 317−323.
(58) Baclayon, M.; Roos, W. H.; Wuite, G. J. L. Sampling Protein Form and Function with the Atomic Force Microscope. *Mol. Cell. Proteomics* **2010**, *9*, 1678−1688.
(59) Longo, G.; Rio, L. M.; Roduit, C.; Trampuz, A.; Bizzini, A.; Dietler, G.; Kasas, S. Force Volume and Stiffness Tomography Investigation on the Dynamics of Stiff Material under Bacterial Membranes. *J. Mol. Recogn.* **2012**, *25*, 278−284.
(60) Günther, T. J.; Suhr, M.; Raff, J.; Pollmann, K. Immobilization of Microorganisms for AFM Studies in Liquids. *RSC Adv.* **2014**, *4*, 51156−51164.
(61) García-Massó, X.; Huber, M. C.; Friedmann, J.; González, L. M.; Schiller, S. M.; Toca-Herrera, J. L. Automated Detection of Protein Unfolding Events in Atomic Force Microscopy Force Curves. *Microsc. Res. Tech.* **2016**, *79*, 1105−1111.
(62) Arfsten, J.; Leupold, S.; Bradtmöller, C.; Kampen, I.; Kwade, A. Atomic Force Microscopy Studies on the Nanomechanical Properties of Saccharomyces Cerevisiae. *Colloids Surf., B* **2010**, *79*, 284−290.
(63) Baniasadi, M.; Xu, Z.; Gandee, L.; Du, Y.; Lu, H.; Zimmern, P.; Minary, M. Nanoindentation of Pseudomonas Aeruginosa Bacterial Biofilm Using Atomic Force Microscopy. *Mater. Res. Express* **2014**, *1*, 045411.
(64) Ivanov, I. E.; Kintz, E. N.; Porter, L. A.; Goldberg, J. B.; Burnham, N. A.; Camesano, T. A. Relating the Physical Properties of Pseudomonas Aeruginosa Lipopolysaccharides to Virulence by Atomic Force Microscopy. *J. Bacteriol.* **2011**, *193*, 1259−1266.
(65) Sullivan, C. J.; Venkataraman, S.; Retterer, S. T.; Allison, D. P.; Doktycz, M. J. Comparison of the Indentation and Elasticity of E. Coli and Its Spheroplasts by AFM. *Ultramicroscopy* **2007**, *107*, 934−942.
(66) Sicard, D.; Cecioni, S.; Iazykov, M.; Chevolot, Y.; Matthews, S. E.; Praly, J.-P.; Souteyrand, E.; Imberty, A.; Vidal, S.; Phaner-Goutorbe, M. AFM Investigation of Pseudomonas Aeruginosa Lectin LecA (PA-IL) Filaments Induced by Multivalent Glycoclusters. *Chem. Commun.* **2011**, *47*, 9483−9485.
(67) Coutable, A.; Thibault, C.; Chalmeau, J.; François, J. M.; Vieu, C.; Noireaux, V.; Trévisiol, E. Preparation of Tethered-Lipid Bilayers on Gold Surfaces for the Incorporation of Integral Membrane Proteins Synthesized by Cell-Free Expression. *Langmuir* **2014**, *30*, 3132−3141.
(68) Kulp, A.; Kuehn, M. J. Biological Functions and Biogenesis of Secreted Bacterial Outer Membrane Vesicles. *Annu. Rev. Microbiol.* **2010**, *64*, 163−184.
(69) Jauvert, E.; Palleau, E.; Dague, E.; Ressier, L. Directed Assembly of Living Pseudomonas Aeruginosa Bacteria on PEI Patterns Generated by Nanoxerography for Statistical AFM Bioexperiments. *ACS Appl. Mater. Interfaces* **2014**, *6*, 21230−21236.
(70) Beckmann, M. A.; Venkataraman, S.; Doktycz, M. J.; Nataro, J. P.; Sullivan, C. J.; Morrell-Falvey, J. L.; Allison, D. P. Measuring Cell Surface Elasticity on Enteroaggregative Escherichia Coli Wild Type and Dispersin Mutant by AFM. *Ultramicroscopy* **2006**, *106*, 695−702.
(71) Vadillo-Rodríguez, V.; Logan, B. E. Localized Attraction Correlates with Bacterial Adhesion to Glass and Metal Oxide Substrata. *Environ. Sci. Technol.* **2006**, *40*, 2983−2988.
(72) He, R.; Di Bonaventura, I.; Visini, R.; Gan, B.-H.; Fu, Y.; Probst, D.; Lüscher, A.; Köhler, T.; van Delden, C.; Stocker, A.; et al. Design, Crystal Structure and Atomic Force Microscopy Study of Thioether Ligated d,l-Cyclic Antimicrobial Peptides against Multidrug Resistant Pseudomonas Aeruginosa. *Chem. Sci.* **2017**, *8*, 7464−7475.
(73) Atabek, A.; Camesano, T. A. Atomic Force Microscopy Study of the Effect of Lipopolysaccharides and Extracellular Polymers on Adhesion of Pseudomonas Aeruginosa. *J. Bacteriol.* **2007**, *189*, 8503−8509.
(74) Gammoudi, I.; Mathelie-guinlet, M.; Morote, F.; Beven, L.; Moynet, D.; Grauby-heywang, C.; Cohen-bouhacina, T. Morphological and Nanostructural Surface Changes in Escherichia Coli over Time, Monitored by Atomic Force Microscopy. *Colloids Surf., B* **2016**, *141*, 355−364.
(75) Vadillo-Rodriguez, V.; Schooling, S. R.; Dutcher, J. R. In Situ Characterization of Differences in the Viscoelastic Response of Individual Gram-Negative and Gram-Positive Bacterial Cells. *J. Bacteriol.* **2009**, *191*, 5518−5525.
(76) Mularski, A.; Wilksch, J. J.; Hanssen, E.; Strugnell, R. A.; Separovic, F. Atomic Force Microscopy of Bacteria Reveals the Mechanobiology of Pore Forming Peptide Action. *Biochim. Biophys. Acta, Biomembr.* **2016**, *1858*, 1091−1098.
(77) Takai, E.; Costa, K. D.; Shaheen, A.; Hung, C. T.; Guo, X. E. Osteoblast Elastic Modulus Measured by Atomic Force Microscopy Is Substrate Dependent. *Ann. Biomed. Eng.* **2005**, *33*, 963−971.
(78) Guragain, M.; King, M. M.; Williamson, K. S.; Pérez-Osorio, A. C.; Akiyama, T.; Khanam, S.; Patrauchan, M. A.; Franklin, M. J. The Pseudomonas aeruginosa PAO1 Two-Component Regulator CarSR Regulates Calcium Homeostasis and Calcium-Induced Virulence Factor Production through Its Regulatory Targets CarO and CarP. *J. Bacteriol.* **2016**, *198*, 951−963.
(79) Sarkisova, S. A.; Lotlikar, S. R.; Guragain, M.; Kubat, R.; Cloud, J.; Franklin, M. J.; Patrauchan, M. A. A Pseudomonas Aeruginosa EF-Hand Protein, EfhP (PA4107), Modulates Stress Responses and Virulence at High Calcium Concentration. *PLoS One* **2014**, *9*, No. e98985.
(80) Dominguez, D. C. Calcium Signalling in Bacteria. *Mol. Microbiol.* **2004**, *54*, 291−297.
(81) Guragain, M.; Lenaburg, D. L.; Moore, F. S.; Reutlinger, I.; Patrauchan, M. A. Calcium Homeostasis in Pseudomonas Aeruginosa Requires Multiple Transporters and Modulates Swarming Motility. *Cell Calcium* **2013**, *54*, 350−361.

DOI: 10.1021/acs.langmuir.8b02079
Langmuir 2018, 34, 10806−10815

(82) Atwater, I.; Dawson, C. M.; Ribalet, B.; Rojas, E. Potassium Permeability Activated by Intracellular Calcium Ion Concentration in the Pancreatic Beta-cell. *J. Physiol.* **1979**, *288*, 575−588.
(83) Duchen, M. R.; Smith, P. A.; Ashcroft, F. M. Substrate-Dependent Changes in Mitochondrial Function, Intracellular Free Calcium Concentration and Membrane Channels in Pancreatic *β*-Cells. *Biochem. J.* **1993**, *294*, 35−42.
(84) Ramstad, S.; Futsaether, C. M.; Johnsson, A. Porphyrin Sensitization and Intracellular Calcium Changes in the Prokaryote Propionibacterium Acnes. *J. Photochem. Photobiol., B* **1997**, *40*, 141−148.
(85) Arlehamn, C. S. L.; Pétrilli, V.; Gross, O.; Tschopp, J.; Evans, T. J. The Role of Potassium in Inflammasome Activation by Bacteria. *J. Biol. Chem.* **2010**, *285*, 10508−10518.
(86) Kaess, F.; Mita, S.; Xie, J.; Reddy, P.; Klump, A.; Hernandez-Balderrama, L. H.; Washiyama, S.; Franke, A.; Kirste, R.; Hoffmann, A.; et al. Correlation between Mobility Collapse and Carbon Impurities in Si-Doped GaN Grown by Low Pressure Metalorganic Chemical Vapor Deposition. *J. Appl. Phys.* **2016**, *120*, 105701.
(87) Hudzicki, J. *Kirby-Bauer Disk Diffusion Susceptibility Test Protocol*; American Society for Microbiology, 2009; pp 1−14.

DOI: 10.1021/acs.langmuir.8b02079
Langmuir 2018, 34, 10806−10815